



Behavior of structural steel moment connections under fire loading

Mina S. Seif¹, Joseph A. Main², Fahim H. Sadek³

Abstract

Performance-based methodologies to evaluate the fire performance of structures are needed to move beyond the prescriptive procedures presently in use. Analytical methods are needed for simulating the performance of structural systems, including connections, subject to realistic fire effects. Framing connections may be subject to large unanticipated deformations and loads during fire events, and connection failure may lead to other failures or local collapse. In this study, the performance of steel moment frames under fire-induced heating was investigated using detailed finite-element modeling. Models of two types of seismically designed steel moment frames were developed, including an intermediate moment frame with welded unreinforced flange, bolted web (WUF-B) connections, and a special moment frame with reduced beam section (RBS) connections. Assemblies consisting of two columns and a single beam span were modeled, with highly refined modeling of the connection regions. Structural analyses were performed under gravity loads in combination with a thermal loading scenario consisting of a heating phase followed by a cooling phase. Recently developed temperature-dependent material models for structural steel and bolts that incorporate erosion-based modeling of fracture were implemented in the study. The influence of axial restraint on the performance of the moment frames was investigated by considering different support conditions for the end columns. Local buckling in the connection region was observed in the heating phase of the analyses, with buckling occurring at lower temperatures under more highly restrained conditions. Subsequent to local buckling, substantial tensile forces were developed in the beams during the cooling phase.

1. Introduction

There is a lack of tools for modeling the response of structural systems, including connections, to realistic, uncontrolled fires. Fire protection of steel structures is usually provided through prescriptive requirements based on the standard fire test (ASTM 2011), which has changed little since it was introduced in 1917. Such tests typically characterize heat transmission through elements and subsystems, but do not provide information about structural performance in real

¹ Research Structural Engineer, National Institute of Standards and Technology (NIST), Gaithersburg, MD, mina.seif@nist.gov

² Research Structural Engineer, National Institute of Standards and Technology (NIST), Gaithersburg, MD, joseph.main@nist.gov

³ Leader, Structures Group, National Institute of Standards and Technology (NIST), Gaithersburg, MD, fahim.sadek@nist.gov

fire. A fuller understanding of the problem will lead to the development of analytical tools and design standards that explicitly consider realistic fire loading for both the design of new buildings and assessment and retrofit of existing ones. Development of design tools for evaluating fire effects requires detailed finite element (FE) analyses that consider all failure modes, including local buckling, at elevated temperatures.

During exposure to fire, large axial compressive and/or tensile forces may develop in floor beams and their connections. A number of researchers have studied the effects of fire on connections, though most of the literature addresses shear connections and semi-rigid connections. Sarraj et al. (2007) developed detailed solid element models for shear tab connections with bolts to evaluate bolt shear and bearing behavior. Yu et al. (2009) performed an experimental investigation of the behavior of shear tab connections subjected to vertical shear and tensile forces at elevated temperatures and measured their moment-rotation capacity. Seif et al. (2013) discussed failure modes of shear-tab connections at elevated temperatures, while Seif et al. (2014) similarly discussed failure modes of moment connections under similar heating conditions. For moment connections, Yang et al. (2009) conducted experiments on welded moment connections where the connections and members immediately adjacent to the connection were heated up to 650 °C and then loaded to failure under an applied moment. Yielding, necking, fracture, bolt shear deformation, and local buckling were observed, and a reduction of member stiffness to 25% of ambient values was reported. Quiel and Garlock (2010) conducted detailed finite element analyses of shear and moment connections for 2D and 3D building frames. Their results indicate that thermal gradients can produce significant changes in the deflection mechanics and plastic P - M limit-state behavior.

This paper presents results from a study employing FE analysis with geometric and material nonlinearities, using solid and shell elements to model the failure modes of typical steel moment connections in response to elevated temperatures. The purpose of the analyses is to gain better understanding and insights into the behavior of moment connections, including failure modes, when subjected to fire exposure and various restraining conditions. Recently developed temperature-dependent material models for different types of steels used in connections are implemented. The results presented illustrate the behavior and failure modes of connections and assemblies under varying load, temperature, and boundary conditions. Ongoing research efforts are focused on developing reduced-order modeling approaches for connections and assemblies that can capture these behaviors and failure modes.

2. Prototype Moment Frames

As described in Lew et al. (2013), the National Institute of Standards and Technology (NIST) worked with a panel of practicing structural engineers across the U.S. to develop a number of prototype steel-frame building designs for use in assessing the robustness of structural systems. The buildings were designed according to the American Society of Civil Engineers 7-02 standard (ASCE 2002) and its referenced material design standards, including the American Institute of Steel Construction (AISC) *Load and Resistance Factor Design Specification for Structural Steel Buildings* (AISC 1999) and the AISC *Seismic Provisions for Structural Steel Buildings* (AISC 2002). These prototype buildings are considered representative of typical construction in the United States, and two types of moment frames from the prototype buildings were selected for analysis in this study. The two types of moment frames include an intermediate moment frame

(IMF) with welded unreinforced flange, bolted web (WUF-B) connections, and a special moment frame (SMF) with reduced beam section (RBS) connections. The assemblies considered in this study were portions of these moment frames consisting of a beam supported on two columns and joined using two moment connections. Fig. 1 shows a sketch of a typical assembly.

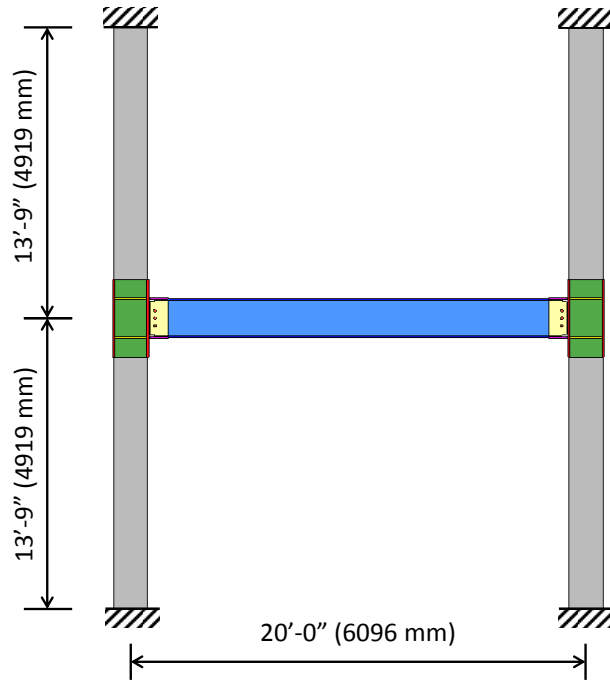


Figure 1. Sketch of a typical assembly.

The moment-frame assembly with WUF-B connections was taken from the second-floor level of a seismically designed IMF in a 10-story prototype building designed for Seismic Design Category C. The WUF-B moment connection is one of the prequalified steel connections listed in FEMA 350 (FEMA 2000), and Fig. 2 shows details of the WUF-B connection used in the IMF assembly considered in this study. The beam flanges are joined to the column flange using complete joint penetration (CJP) groove welds. ASTM A992 structural steel, with an ambient-temperature nominal specified yield strength of $F_{y0} = 50$ ksi (344.8 MPa) was used in all beams and columns. ASTM A36 steel, with $F_{y0} = 36$ ksi (248.2 MPa) was used for the shear tabs and continuity plates at the beam-column connections. ASTM A490 bolts, with $F_{y0} = 130$ ksi (896 MPa), were used to connect the shear tab to the beam web.

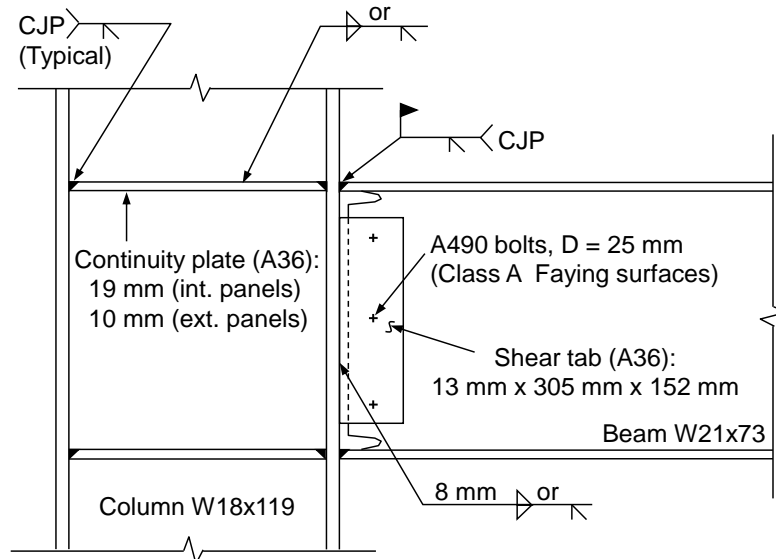


Figure 2. Details of WUF-B moment connection.

Similarly, the moment-frame assembly with RBS connections was taken from the second-floor level of a seismically designed SMF in a 10-story prototype building designed for Seismic Design Category D. The RBS moment connection is also one of the prequalified steel connections listed in FEMA 350 (FEMA 2000). The RBS connection is created by cutting away a portion of the top and bottom flanges of the beam at a distance from the beam-column interface so that yielding is concentrated in this reduced area. Therefore, the reduced section acts as a structural fuse to protect the connection against premature fracture. Fig. 3 shows details of the RBS connection used in the SMF assembly considered in this study. ASTM A992 structural steel was used for the beams and columns.

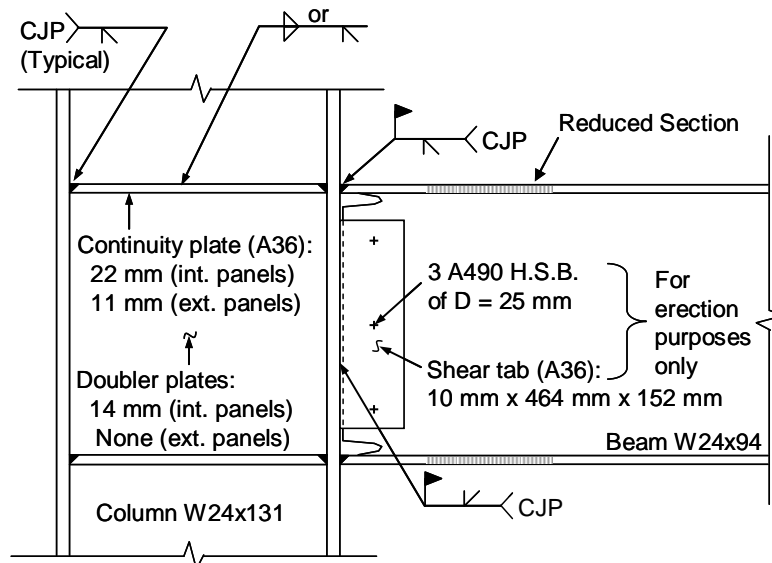


Figure 3. Details of WUF-B moment connection.

3. Modeling and Analysis of Moment-Frame Assemblies

Detailed nonlinear FE analyses were conducted to simulate the behavior and failure modes of the moment-frame assemblies under elevated temperatures. All analyses were performed using explicit time integration in LS-DYNA (LSTC 2012). In each analysis, the assembly was subjected to a uniform gravity load along the beam (applied along the centerline of the top flange), as well as a prescribed temperature time history for the beam and connections. The columns were unheated. The gravity load applied to the beam is from a 1.2(Dead Load) + 0.5(Live Load) combination of 113 psf (5.41 kPa) on the adjacent slabs (refer to Main and Sadek (2012) for a discussion of gravity loads on the prototype buildings). The gravity load was gradually applied over 0.5 seconds to avoid any dynamic amplification. The temperature time history, which is illustrated in Fig. 4, included both a heating phase and a cooling phase. The temperature was gradually ramped up from ambient temperature (20 °C) to a peak temperature, was held constant at the peak temperature, and then was dropped back to ambient temperature. Most analyses considered a uniform temperature for the beams and connections, with a peak temperature of 700 °C, while specific analyses considered the influence of a temperature gradient through the beam depth and of heating to a lower peak temperature. Different restraint conditions for the columns at beam level were also considered, and details of the specific analysis cases considered are presented in Section 5.

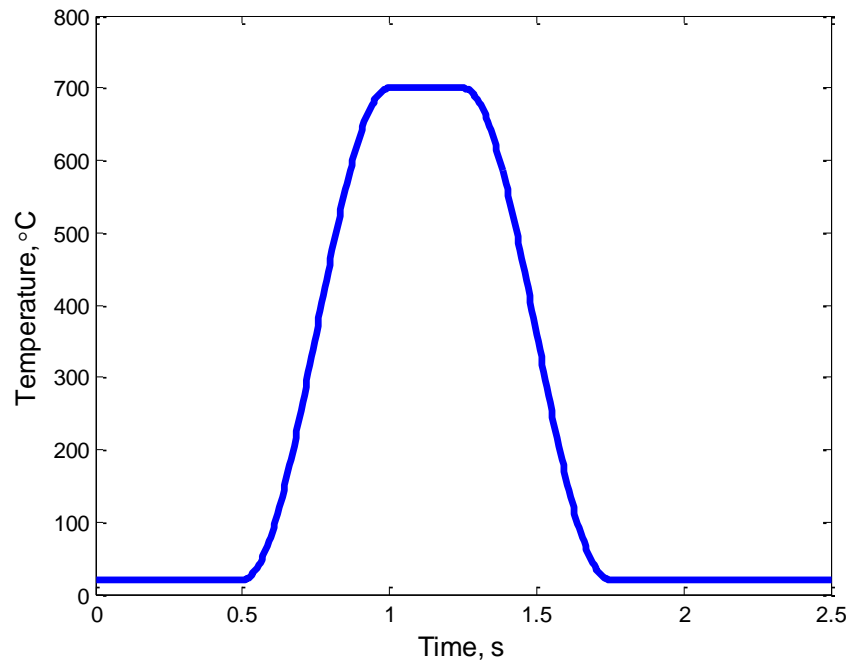


Figure 4. Temperature loading profile.

The WUF-B connections in the IMF assembly (Fig. 1) were modeled using finely meshed three-dimensional solid elements for the beam, bolts, and shear tab, as shown in Fig. 5. Fully integrated eight-node solid elements were used. A typical element size of 0.12 in (3 mm) was used for the beam and the shear tab. A finer mesh with a typical element size of 0.06 in (1.5 mm) was used for the bolts. Contact was defined between the bolts, shear tab, and beam web to model the transfer of forces through the bolted connection, including friction, with a value of 0.3

assumed for both the static and dynamic coefficients of friction. No pre-tension in the bolts was considered in the analyses, because experimental and computational results have shown that pre-tension slightly affects the initial response of a bolt in shear but does not significantly affect the ultimate behavior or fracture of the bolt. To model fracture, element erosion was activated for the solid elements, as discussed in the following section. Outside of the connection regions, the beams and columns were modeled using shell elements, and nodal constraints were used to enforce continuity of displacements and rotations at the interfaces between the solid and shell elements.

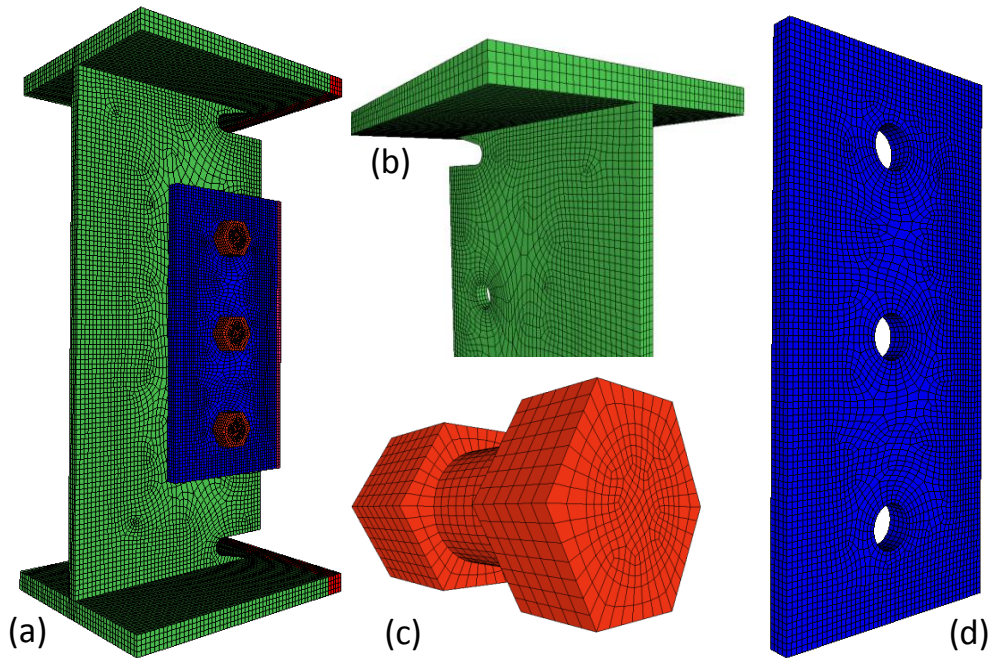


Figure 5. Detailed model of the WUF-B connection: (a) full model, (b) beam, (c) bolt, and (d) shear tab.

The RBS connections in the SMF assembly (Fig. 2) were modeled using finely meshed two-dimensional shell elements, as shown in Fig. 6. The reduced section of the beam was modeled using a fine shell element mesh with element size of about 0.25 in (6.4 mm). Away from the reduced section, a coarser mesh was used, with an element size of about 1 in (25.4 mm). Fully integrated four-node shell elements were used. Element erosion was not activated for the shell elements, and thus fracture was not considered in the analyses. Future analyses will consider fracture modeling using shell elements, which will require calibration of erosion strain values that depend on both temperature and mesh size, as discussed for solid elements in the following section. The following section discusses the temperature-dependent material models used for the various components of the assemblies at elevated temperatures.

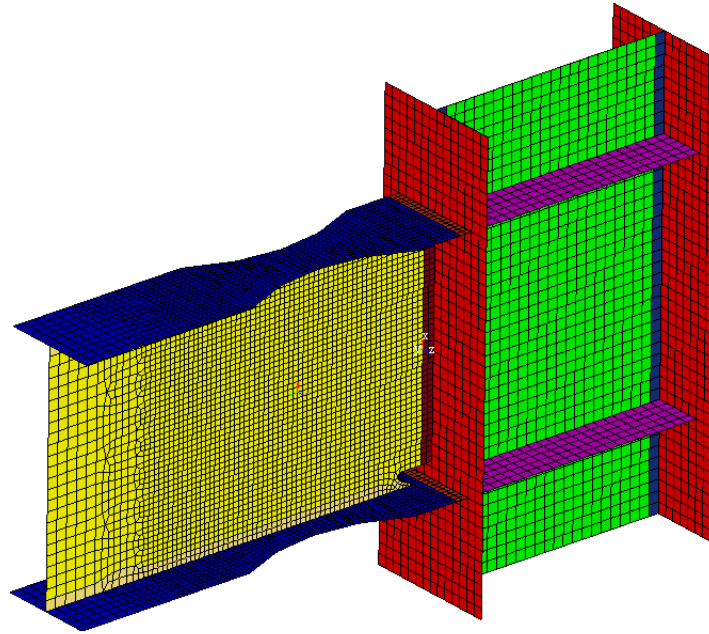


Figure 6. Detailed model of the RBS connection.

4. Temperature-Dependent Material Modeling

A key issue in evaluating the response of structural systems to fire effects is the representation of material behavior at elevated temperatures. In addition to stress-strain behavior, modeling of fracture is required to capture failure modes such as tear-out in connection plates and bolt shear rupture. The use of explicit finite element software packages allows for modeling of sequential failures, including fracture. Fracture can be simulated using element erosion, in which elements are removed from the analysis when specified failure criteria are satisfied. However, the basis for determining and implementing material failure criteria at elevated temperatures is not well-established in the literature. This section summarizes a finite element material modeling methodology for structural steels at elevated temperatures including erosion-based modeling of fracture, developed by Seif et al. (2015). A recently developed temperature-dependent material model for structural steels was combined with a plastic strain-based failure criterion for element erosion. Using finite element models of tensile coupons, this failure criterion was calibrated against experimental data on elongation at fracture, and the influence of temperature and mesh size on the failure criterion was investigated.

Luecke et al. (2013) developed an empirical model that provides temperature dependent material models for different structural steels. The model is based on experiments conducted at the National Institute of Standards and Technology (NIST) and published data from numerous experiments reported in the literature. The model accounts for the change in yield strength and post-yield strain hardening with temperature. However, the model does not account for creep effects. Relationships for true stress and true strain are required to define material models in LS-DYNA analyses. However, as is discussed subsequently, detailed finite element models of tensile coupons are used to obtain engineering stress-strain curves for comparison with experimental measurements, particularly regarding the post-ultimate behavior, including necking and fracture.

Experimental data to support temperature-dependent material properties for structural bolts are more limited than for structural steel, particularly data regarding the temperature-dependence of deformations or elongations at fracture. Much of the available experimental data for bolt shear tests is influenced by deformation of the shear loading assembly, making it difficult to isolate the bolt performance. Given these limitations, an interim approach for modeling the temperature-dependent nonlinear material behavior and fracture of bolts is described below.

4.1 Structural Steel

For structural steel (beams, columns, and shear tabs), the yield strength F_y and the elastic modulus E are temperature-dependent, and are expressed as functions of temperature. The true stress σ_{true} is expressed as a function of true strain ϵ_{true} , for three different regions: (a) linear up to the yielding stress, followed by (b) a power law expression up to the tensile stress, and finally (c) extending tangentially until fracture. The dependence of the stress-strain relationship on temperature is assumed to be the same whether the material is being heated or cooled.

It is noted that the power law equation was calibrated to match available experimental data up to the tensile strength, and special care is needed in modeling the post-ultimate material behavior, including necking and fracture. Seif et al. (2015) developed an approach for modeling the post-ultimate behavior of structural steel at elevated temperatures, by using element erosion to represent fracture. The onset of erosion was calibrated to match available experimental data of fracture in coupons at elevated temperatures. The failure criterion used for element erosion is based on the effective plastic strain, a scalar measure of plastic strain that incorporates its various tensor components. Element erosion is activated when the effective plastic strain in any element (i.e., the local plastic strain in a section or component) exceeds a specified critical value, called the erosion strain ϵ_{er} . Analyses of detailed, three-dimensional solid element models tensile coupons were conducted to calibrate the erosion strain values against available experimental data on elongation of tensile coupons, including data for ASTM A992 steel from Hu and Morovat (2009) and data for ASTM A572 Grade 50 steel from Luecke (2005). Temperature-dependent values of the erosion strain were used to achieve the best agreement with the experimental data.

To illustrate the modeling of post-ultimate necking and fracture, Fig. 7 shows analysis results from uniaxial extension of a tensile coupon at 500 °C. Engineering strain values in the stress-strain curve of Fig. 7 were calculated based on the relative displacement of two nodes at the ends of the gauge section, with an initial length of $G_o = 1$ in (25.4 mm). Contours of effective plastic strain are also shown in Fig. 7 at different points labeled along the computed stress-strain curve. Points *a* and *b* are prior to the onset of necking, and the corresponding plastic strain contours show fairly uniform plastic strain values along the gauge length that are comparable to the corresponding engineering strain values. For example, point *a* corresponds to an engineering strain of 0.1, and comparable plastic strains of about 0.1 are observed. However, points *c* and *d* are after the onset of necking, and the contours of plastic strain clearly indicate localization of strain near the center of the gauge length, with plastic strain values significantly exceeding the corresponding engineering strain. For example, point *d* (just prior to fracture) corresponds to an engineering strain of 0.35, but larger plastic strains of about 0.39 are observed in the necking region. Because of this localization of plastic strain that occurs during necking, erosion strain values are generally larger than the engineering strain values at which fracture occurs. An

erosion strain of $\epsilon_{er} = 0.40$ was used for the analysis in Fig. 7 to achieve fracture at an engineering strain of 0.35.

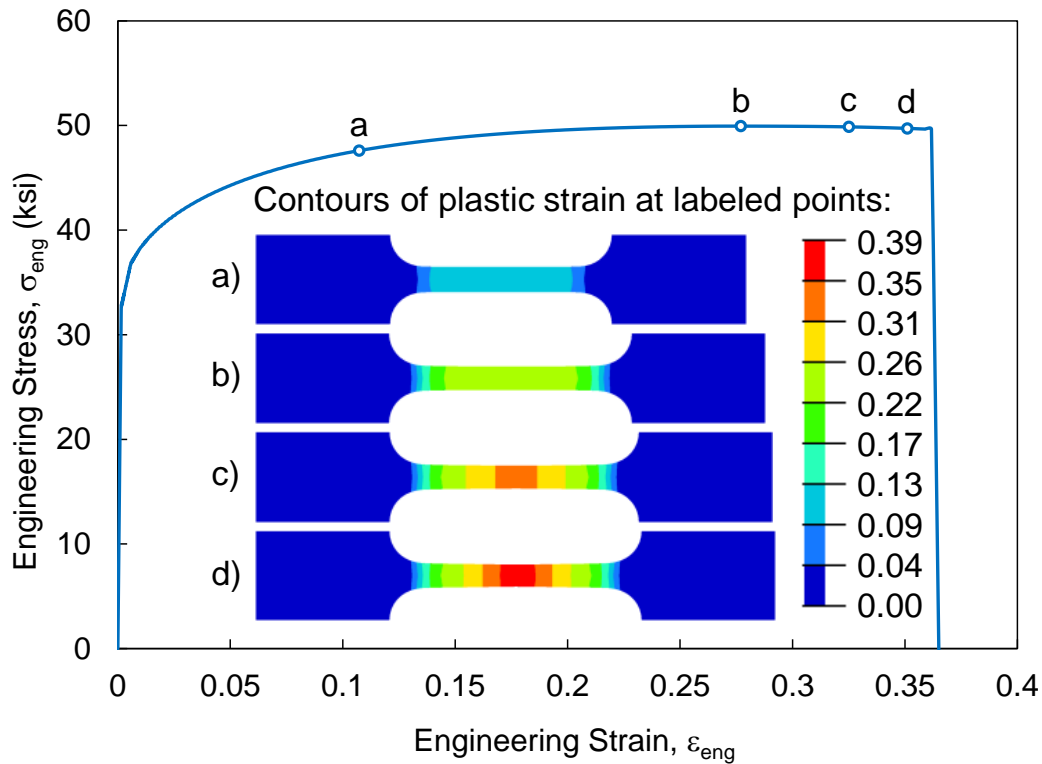


Figure 7. FE analysis results for a tensile coupon model at 500 °C (1 ksi = 6.895 MPa).

Fig. 8 shows the engineering stress-strain curves obtained from FE analysis of tensile coupons at temperatures of 20 °C, 400 °C, 500 °C, and 600 °C, using the proposed material modeling approach with erosion strain values calibrated against experimental data. The engineering strain at fracture is largest at 20 °C and reaches a minimum value at 500 °C before increasing again at 600 °C. Because of the lack of experimental data in the literature regarding the effect of elevated temperatures on the strain at fracture of A36 steel (from which the shear tabs are typically constructed), the values of ϵ_{er} were assumed to be equal to those of the A992 steel for the purpose of the analyses. Since the ASTM specifications require A36 steel to sustain greater elongations than A992 steel, this assumption would tend to predict premature fracture for the A36 steel. However, this assumption did not affect the results, as fracture did not occur in the shear tabs.

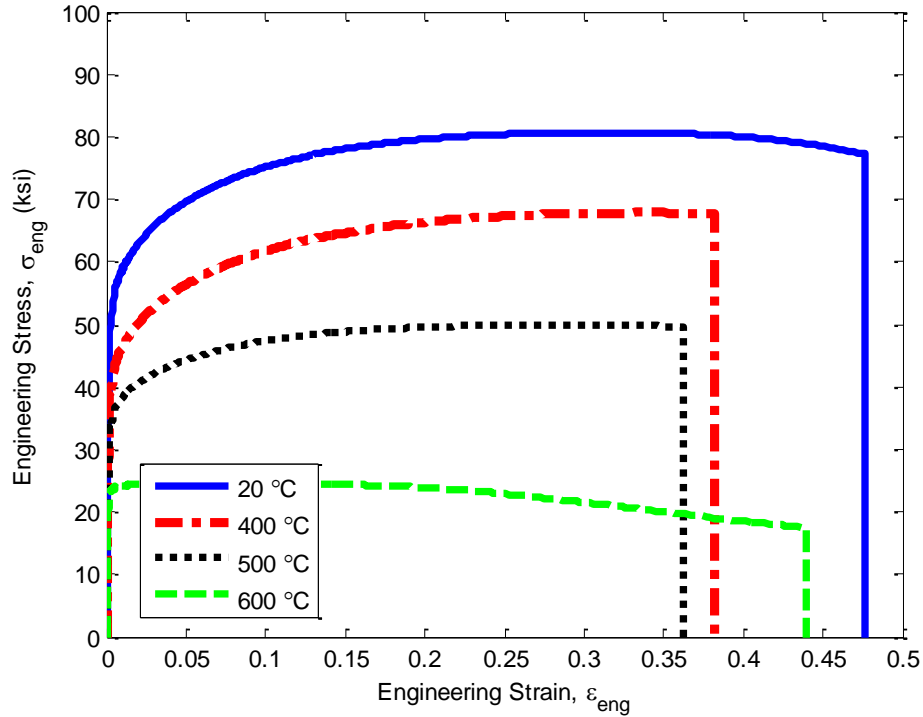


Figure 8. Target values of engineering strain at fracture determined from experimental data.

4.2 Bolts

For A490 high-strength bolts, the yield strength F_y , elastic modulus E , and ultimate strength F_u are also temperature-dependent. However, compared to rolled steel, bolts sustain their F_y value with the increase of temperature up to about 400 °C, after which it drops dramatically. At 400 °C, both rolled steel and bolts sustain about 80 % of their yield capacity. At 600 °C, rolled steel sustains about half of its yield capacity, while bolts have lost more than 82 % of their yield capacity.

A tri-linear stress-strain relationship is developed and used, with regions: (i) up to yield strain, (ii) from yield till ultimate strain, and (iii) from ultimate strain till fracture. The temperature-dependent ultimate strain, $\epsilon_u(T)$, is assumed to have a value of 0.1 at 20°C and to decrease linearly with temperature to a value of 0.05 at 600 °C. The dependence of the stress-strain relationship on temperature is assumed to be the same whether the material is being heated or cooled.

Similar to rolled steel, the failure criterion used for element erosion is based on the effective plastic strain. Element erosion is activated when the effective plastic strain in any element exceeds ϵ_{er} . The erosion strain is temperature-dependent and based on analyses of detailed, three-dimensional solid-element models A490 steel bolts. The values of ϵ_{er} were calibrated against available tensile experimental data from Kodur et al. (2012). To determine the appropriate value of erosion strain at each temperature, the erosion strain was adjusted until the resulting engineering strain at fracture matched a target value determined from the available experimental data.

The material model for structural bolts and the associated erosion strain values were developed and calibrated on the basis of tensile test data, but it is important that the modeling approach is also capable of capturing the behavior and failure of structural bolts in shear. To verify the adequacy of the modeling approach in representing shear behavior, FE analyses were performed on a series of double-shear bolt tests. Solid-element models of double-shear test specimens were developed with dimensions corresponding to tests conducted by Wallaert and Fisher (1965) at ambient temperature. ASTM A36 steel was used for the bearing plates, which has comparable properties to the A440 steel used in the tests. Due to symmetry, only half of each specimen was modeled, with boundary conditions reflecting the symmetry as shown in Fig. 9(a). The center plate was subjected to tensile loading in the analysis, which subjected the bolts to double shear until fracture across the bolt occurred. Fracture initiated when the effective plastic strain in any element reached the specified erosion strain, ϵ_{er} , as discussed in previous sections. Fig. 9(b) shows the solid-element mesh of the bolt after shear fracture.

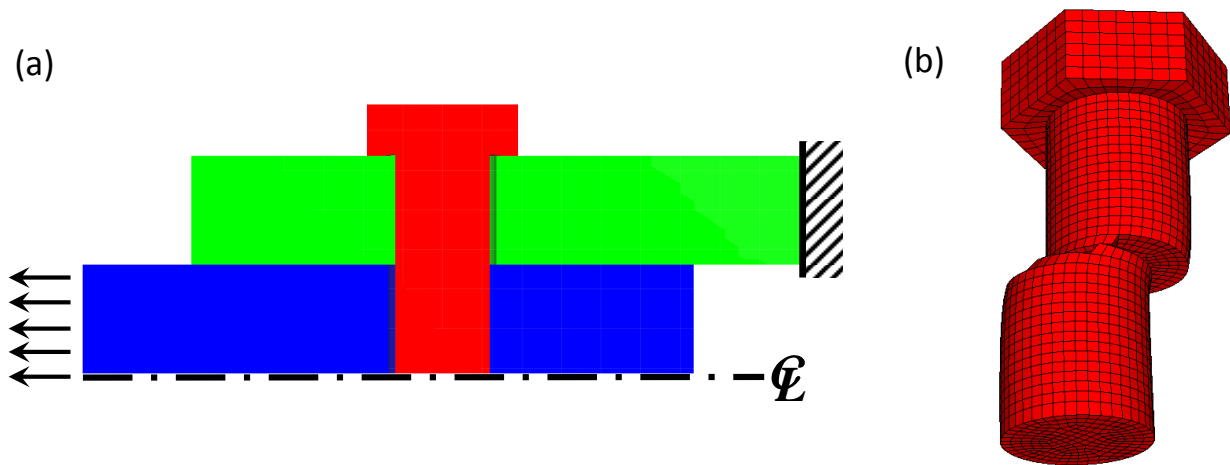


Figure 9. Detailed model of a double-shear bolt test: (a) section view, (b) bolt after fracture.

Using the proposed modeling approach for structural bolts, Fig. 10 shows shear stress vs. deformation curves for bolt shear failure from the FE analyses at 20 °C, 400 °C, 500 °C, and 600 °C, for the A490 bolts. The FE results compared reasonably well with experimental results at ambient temperature (not shown in Fig. 10), particularly for the shear stress at fracture. The test specimen sustained somewhat larger deformations than the FE model before fracture, likely due to the deformations of the plates during the experiment. The shear capacity obtained from the FE model for the A490 bolts at ambient temperature was 96 ksi (660 MPa), within 2% of the nominal shear capacity of 94 ksi (646 MPa) specified by Research Council on Structural Connections RCSC (2004).

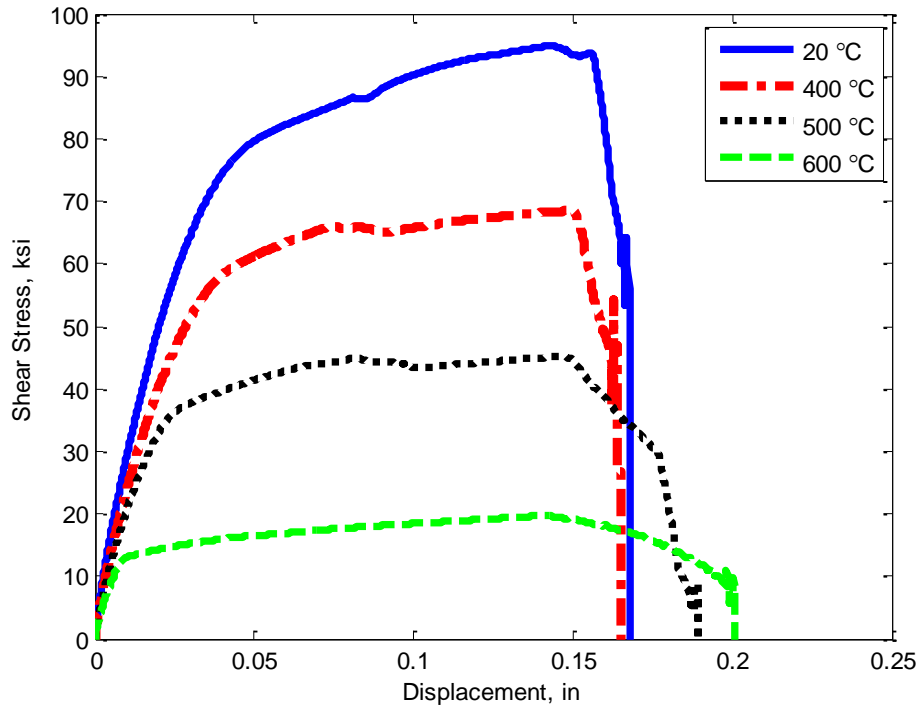


Figure 10. FE results for shear displacement of an A490 bolt at selected temperatures (1 ksi = 6.895 MPa, 1 in = 254 mm).

5. Results and Discussion

The discussion in this section focuses on the behavior and failure modes of the moment-frame assemblies.

5.1 IMF assembly

As illustrated in Fig. 11, three cases are considered for the IMF assembly with WUF-B connections: (a) an assembly with fully constrained beam ends (assuming perfect rigidity of adjacent spans), (b) an assembly with unconstrained beam ends (assuming no adjacent spans), and (c) a three-span assembly (with the outer bays modeled using beam elements and reduced-order connection models and kept at ambient temperature). Fig. 12 shows the axial force in the beam plotted against the prescribed temperature for each of these three analysis cases. The results for each case are discussed in the following sections.

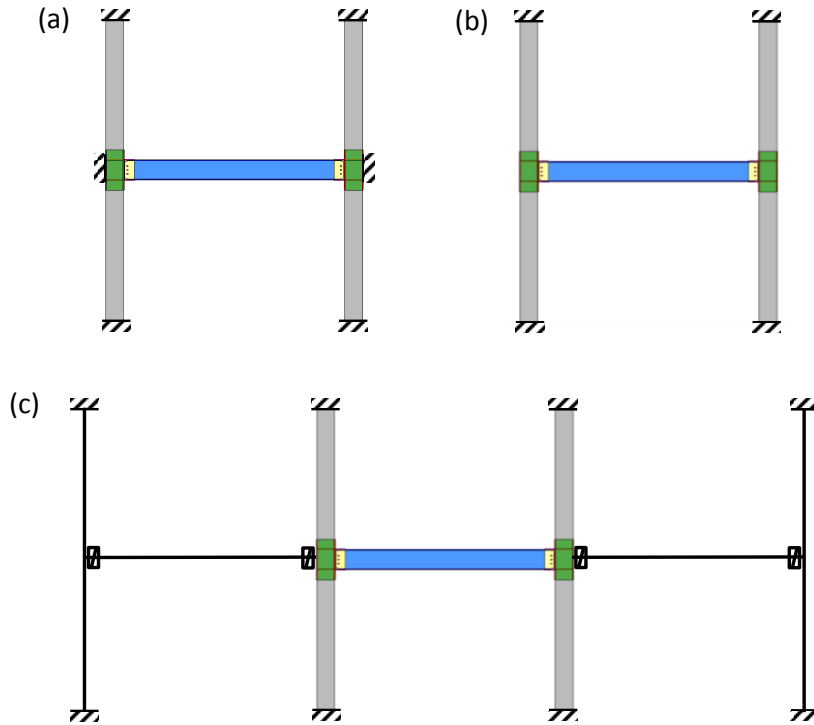


Figure 11. Column restraint cases considered for the IMF assembly: (a) fully constrained, (b) unconstrained, and (c) three-span.

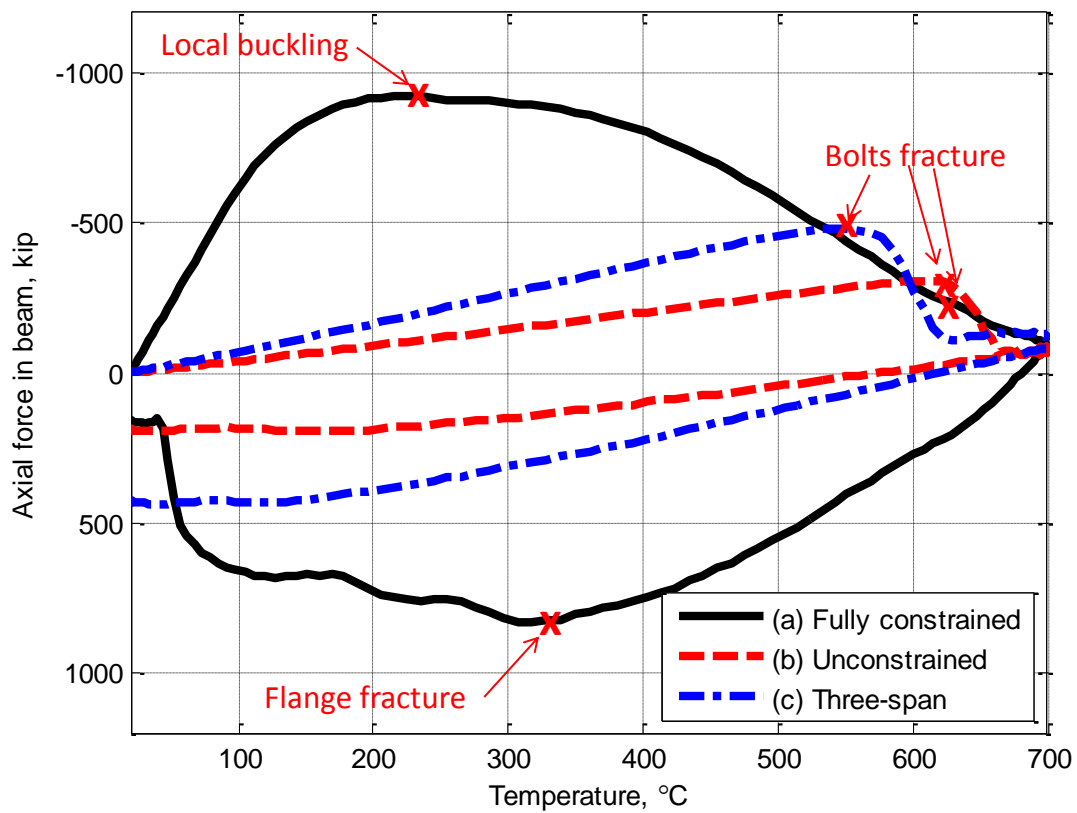


Figure 12. Axial forces in the beam versus temperature for the different WUF-B assembly cases. (1 kip = 4.448 kN)

5.1.1 Fully constrained assembly

For the case of the fully constrained assembly, the beam was not allowed to expand beyond its original length. This led to high axial compressive forces in the beam and connections at relatively low temperatures in the heating phase. Fig. 13 shows the axial force in the beam plotted against the analysis time, in which the heating and cooling phases can be clearly identified through comparison with the prescribed temperature time history shown in Fig. 4. However, in order to clearly illustrate the effect of temperature on the behavior of the assembly, it is preferable to plot the axial force in the beam directly against the corresponding temperature, as in Fig. 12.

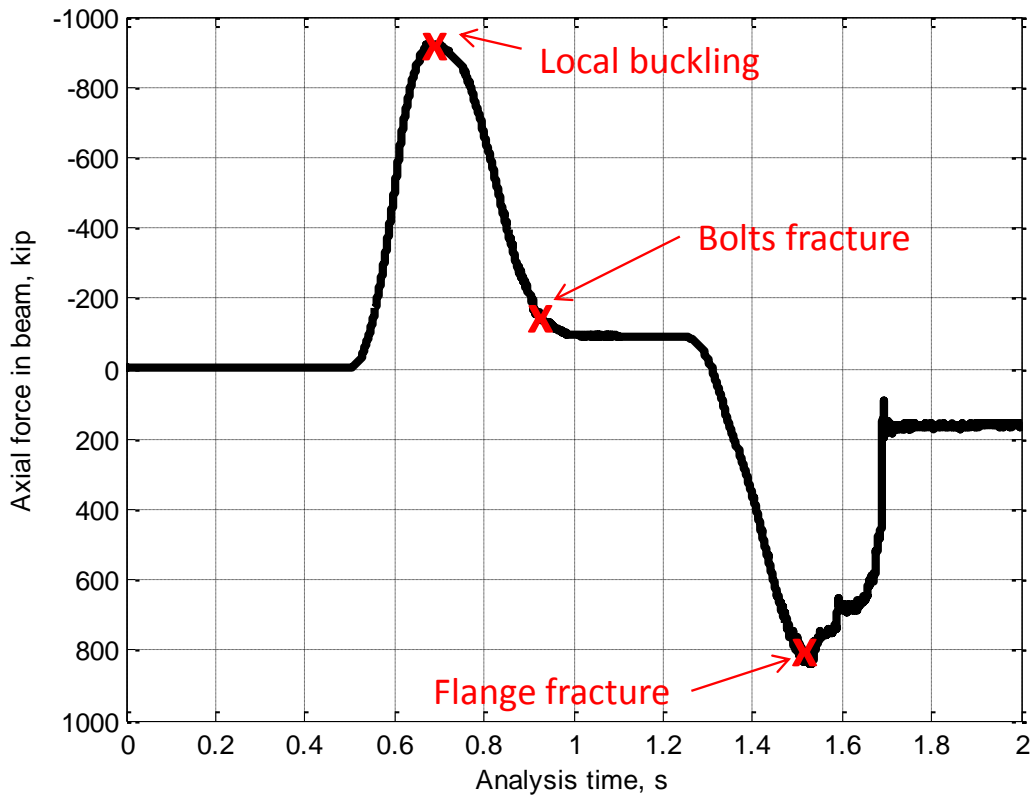


Figure 13. Cross-sectional longitudinal forces in the beam versus the analysis time, for the fully constrained WUF-B assembly.
(1 kip = 4.448 kN)

As shown in Fig. 12, the compressive axial force in the beam reached a peak value of about 927 kip (4124 kN), at only 235 °C. At this point, the connection failed in a local buckling mode, relieving the axial compression in the beam. As the beam continued to heat, the buckled connection deformations increased and the forces in the beam continued to decrease. When the temperature reached about 615 °C, the bolts fractured in shear, and the load continued to decrease until it reached about 10 % of its peak value at 700 °C. Fig. 14 shows the local buckling mode of the connection at the end of the heating phase of the analysis for the fully constrained WUF-B assembly.

In the cooling phase, the axial compression in the beam reversed into high tensile forces, partially reversing the buckled connection deformations. The axial tension in the beam reached a peak of about 836 kip (3719 kN) as the beam cooled to about 305 °C, triggering partial fracture of both the upper and lower flanges in the connection area. However, the partially fractured flanges were able to sustain the applied gravity loads throughout the analysis without collapsing.

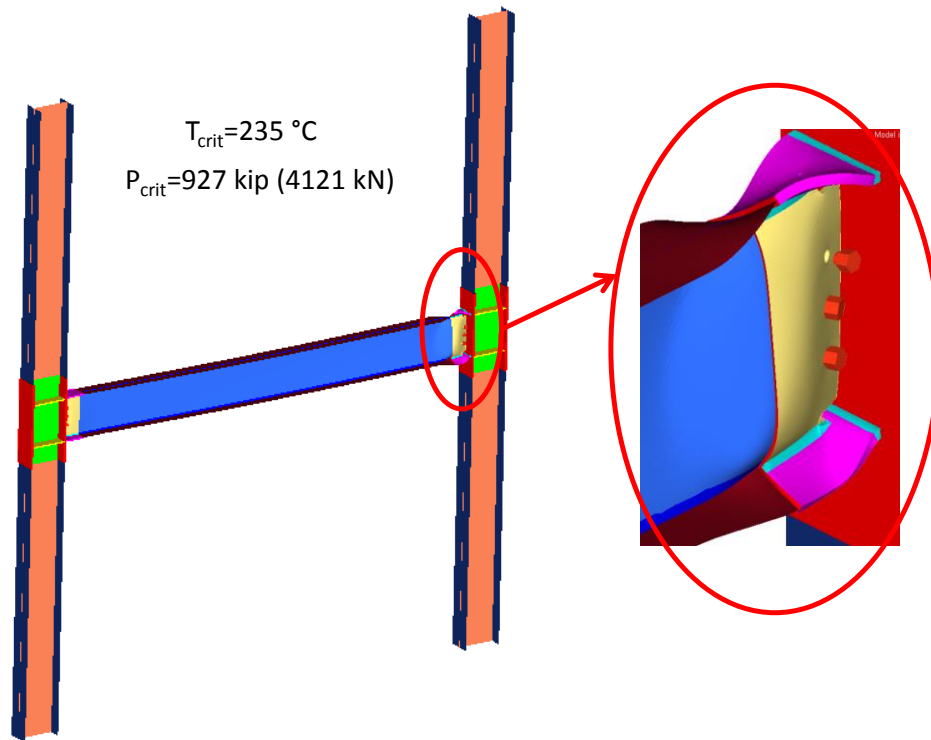


Figure 14. Local buckling mode of the connection at the end of the heating phase of the analysis of the fully constrained WUF-B assembly.

5.1.2 Unconstrained assembly

For the unconstrained assembly case, the beams were allowed to expand as they were only constrained by the stiffness of the columns (as a one-span assembly, with no beam continuity). Compared to the fully constrained assembly, this case led to much lower compressive forces in the beam and connections, at relatively higher temperatures in the heating phase. As seen in Fig. 12, the compressive axial force in the beam reached a peak value of only 310 kip (1379 kN) at 615 °C, roughly one third of the force at three times the temperature compared to the fully constrained case. At this point, the bolts in the connection failed due to shear fracture, relieving the axial compression in the beam, and the beam's flanges deformed under gravity loads, as shown in Fig. 15. In the cooling phase, the axial compression in the beam reversed into tensile forces, partially reversing the flange deformations. The axial tension in the beam reached a peak of about 200 kip (890 kN) as the beam cooled (about 24 % of the peak tensile force reached in the fully constrained case).

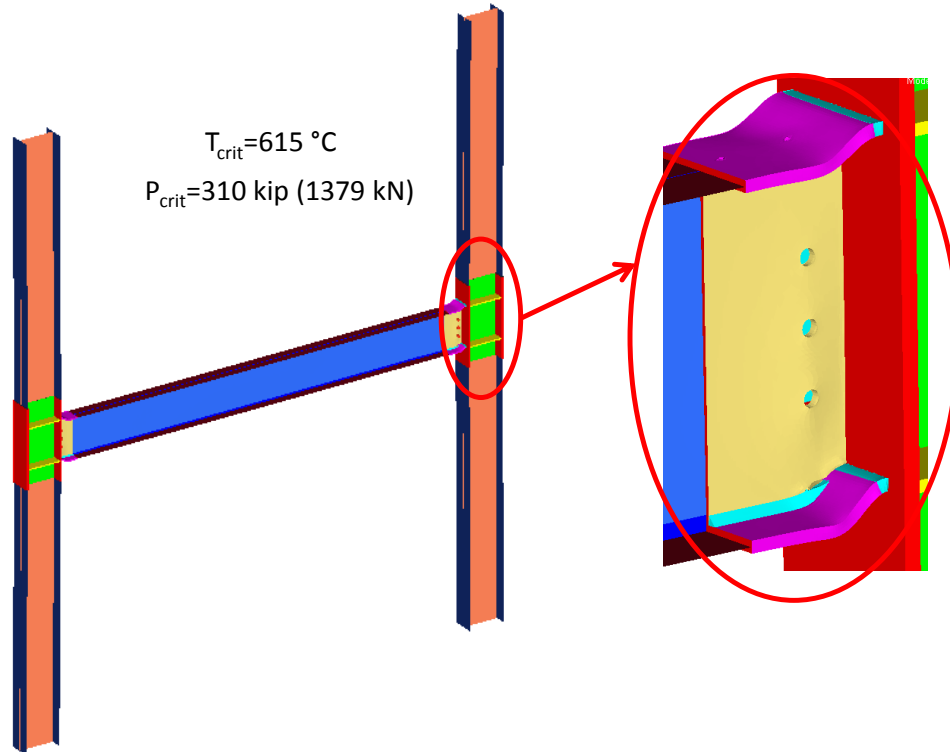


Figure 15. Failure mode of the connection at the end of the heating phase of the analysis of the unconstrained WUF-B assembly.

5.1.3 Three-span assembly

A three-span assembly, as illustrated in Fig. 11(c), was studied as an intermediate case between the fully constrained and the unconstrained assemblies. Gravity loads and prescribed temperature were only applied to the center span. The outer spans were included to more realistically capture the influence of adjoining framing in restraining thermal expansion. The three-span assembly exhibited the same failure mode as the unconstrained assembly, with the bolts fracturing in shear and the flanges deforming under gravity loads (see Fig. 15). However, as expected, higher compressive forces were generated in the beam and connections at slightly lower temperatures in the heating phase. As seen in Fig. 12, the axial compression in the beam reached 483 kip (2149 kN) at 540 °C, roughly 55 % higher force at 10 % lower temperature, compared to the fully constrained case. In the cooling phase, the axial compression again reversed into tensile forces, reaching a peak of about 420 kip (1868 kN) as the beam cooled (more than double the peak tensile force in the unconstrained case).

5.2 SMF assembly

As listed in Table 1, four cases were considered for the SMF assembly with RBS connections: (a) an assembly with fully constrained beam ends (assuming rigid beams on adjacent spans, similar to the sketch in Fig. 11a), (b) an assembly with unconstrained beam ends (assuming no continuity of beam, similar to the sketch in Fig. 11b), (c) an unconstrained assembly that was heated to a pre-buckling temperature prior to cooling, and (d) an unconstrained assembly heated with a temperature gradient across the cross-section. Fig. 16 shows the axial force in the beam plotted against the prescribed temperature for all cases except (d). Each case is discussed in

detail in the following sections. It is noted that the gravity load was sustained in all cases without collapse.

Table 1. Analysis cases considered for the SMF assembly.

| Case | Beam end support | Thermal loading |
|------|-------------------|----------------------------------|
| (a) | Fully constrained | Heated to 700 °C |
| (b) | Unconstrained | Heated to 700 °C |
| (c) | Unconstrained | Heated to 550 °C (pre-buckling) |
| (d) | Unconstrained | Heated to 700 °C (with gradient) |

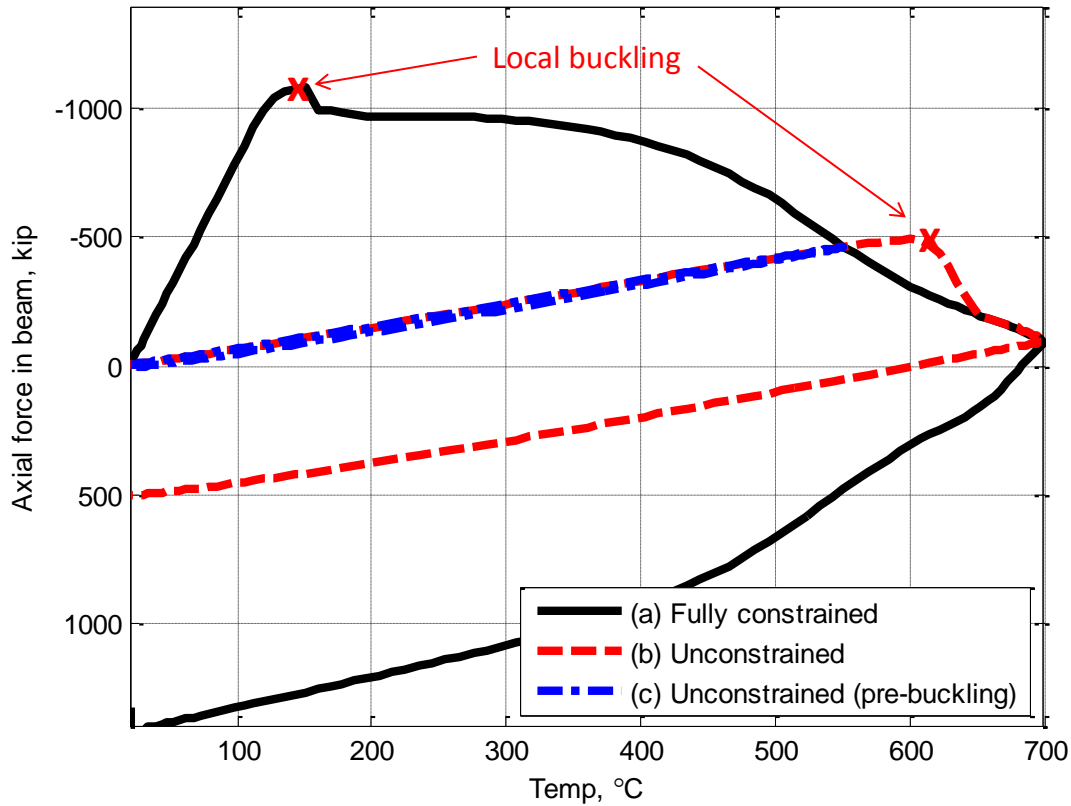


Figure 16. Axial force in the beam versus the temperature for the different RBS assembly cases. (1 kip = 4.448 kN)

5.2.1 Fully constrained assembly

As noted previously for the IMF assembly, in the fully constrained case, the beam in the SMF assembly was not allowed to expand beyond its original length. This led to very high compressive forces in the beam and connections at relatively low temperatures in the heating phase. As seen in Fig. 16, the axial compression in the beam reached a peak value of about 1086 kip (4831 kN) at only 143 °C. That is an 18 % higher force at a 33 % lower temperature than the similar assembly with the WUF-B connections. At this point, the RBS connection failed in a local buckling mode, relieving the axial compression in the beam. As the beam continued to heat, the buckled connection displacements increased and the axial force in the beam continued to decrease until it reached about 10 % of its peak load at 700 °C, similar to the IMF assembly.

Fig. 17(a) shows the buckling failure mode of the RBS connection at the end of the heating phase in the analysis of the fully constrained assembly.

In the cooling phase, the axial compression reversed into high tensile forces, partially reversing the buckled connection deformations. The axial tension reached a peak value of about 1400 kip (6228 kN) as the beam cooled to ambient temperature. As noted previously, element erosion was not activated for the shell elements in the model of the SMF assembly. If element erosion had been activated for modeling of fracture, it is possible that fracture may have occurred in the cooling phase, as was observed for the fully restrained IMF assembly. This possibility will be considered in future analyses.

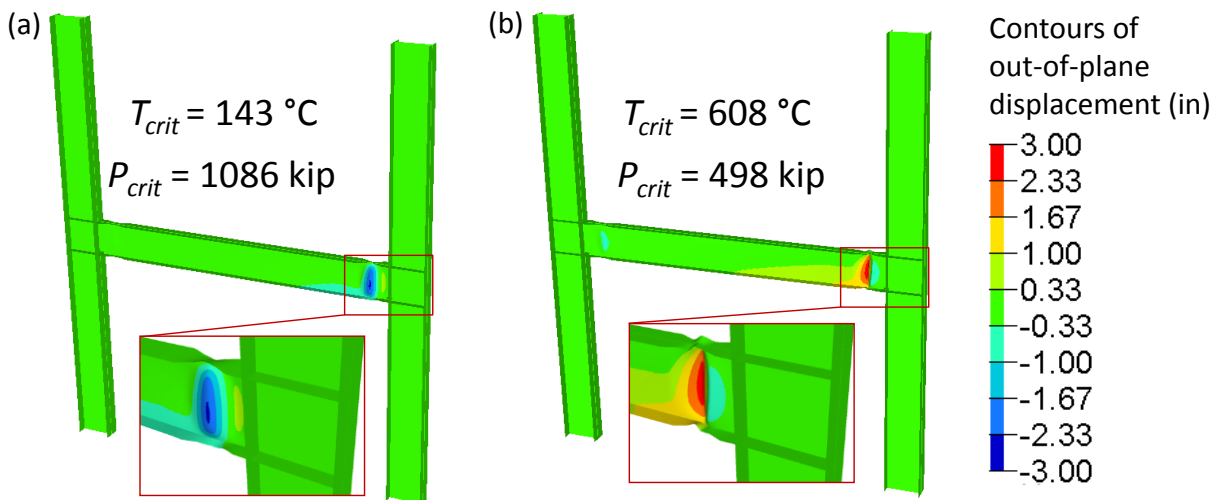


Figure 17. Buckling failure mode of RBS connections at the end of the heating phase for the SMF assembly: (a) fully restrained assembly; (b) unconstrained assembly. (1 in = 25.4 mm)

5.2.2 Unconstrained assembly

The unconstrained SMF assembly exhibited the same failure mode as the fully constrained assembly, as illustrated in Fig. 17(b). However, as expected, much lower compressive forces were generated in the beam and connections at higher temperatures in the heating phase. As seen in Fig. 16, the axial compression in the beam reached a peak value of 498 kip (2215 kN) at 608 °C, roughly half the force at four times the temperature compared to the fully constrained case. Again, in the cooling phase, the axial compression reversed into tensile forces. The axial tension reached a peak value of about 500 kip (2224 kN) at the end of the cooling phase, roughly one third of the peak axial tension generated in the fully constrained case.

5.2.3 Unconstrained assembly, heated to pre-buckling temperature

After analyzing the unconstrained SMF assembly (b), in which the RBS connection buckled at 608 °C, the same case was reanalyzed using a temperature time history with the same basic form but with a peak temperature of 550 °C (just below the buckling temperature). As expected, the connections in this case did not buckle and developed negligible plastic deformations. The axial compression in the beam increased linearly with temperature up to a peak value of 462 kip (2055 kN) at the end of the heating phase, and then dropped linearly to approximately zero at the end of the cooling phase, as seen in Fig. 16. This demonstrates that axial tension does not

develop in the cooling phase unless plastic deformations associated with connection damage develop first in the heating phase.

5.2.4 Unconstrained assembly, with gradient temperature

The unconstrained SMF assembly was analyzed with a temperature gradient through the cross-section, which may be a more realistic temperature distribution when heat conduction can occur from the top flange into the cooler floor slab above. The same time history profile shown in Fig. 4 was used. However, the temperature reached the 700 °C only at the bottom flange. An approximately linear profile through the depth was assumed, reaching only 200 °C at the top flange. Fig. 18 shows the axial force in the beam plotted against the bottom-flange temperature for this case. Similar to the unconstrained SMF assembly with uniform temperature distribution [Fig. 17(b)], the assembly with the gradient distribution failed through local buckling of the RBS connection. However, in the gradient-temperature case, the peak axial compression developed in the beam during the heating phase was only 220 kip (979 kN) at 415 °C, less than half of the compressive force developed in the uniform-temperature case. The axial compressive forces were smaller because the cooler upper portion of the beam had less thermal expansion than in the uniform-temperature case. In the cooling phase, the axial compression again reversed into tensile forces. The peak axial tension in the cooling phase was about 140 kip (623 kN), roughly 28 % of the peak tension in the uniform temperature case.

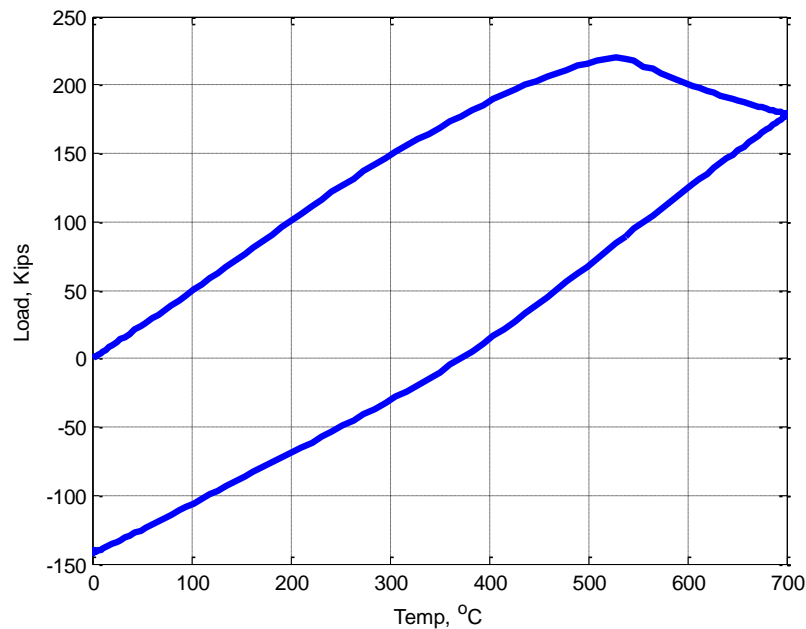


Figure 18. Cross-sectional longitudinal forces in the beam versus the temperature for the unconstrained RBS assembly, heated with a gradient temperature profile through the cross-section of the beam.

6. Concluding Remarks

This paper presented a detailed finite-element approach developed to analyze the behavior and failure modes of seismically designed steel moment frames subjected to elevated temperatures. Finite-element models were developed of two moment-frame assemblies, which included an intermediate moment frame with welded unreinforced flange, bolted web (WUF-B) connections and a special moment frame with reduced beam section (RBS) connections. Both models

incorporated temperature-dependent material models for structural steel and structural bolts. The model of the WUF-B assembly also incorporated erosion-based failure criteria to simulate fracture.

Each moment-frame assembly model was subjected to a uniform gravity load along the beam in conjunction with a prescribed temperature time history. The prescribed temperature history included both a heating phase and a cooling phase, in which the temperature was ramped up from ambient temperature (20 °C) to a peak temperature (700 °C in most cases), was held constant at the peak temperature, and was then dropped back to ambient temperature.

The effects of elevated temperature on the behavior and failure modes of WUF-B and RBS moment-frame assemblies were presented in this paper, and the following observations were made:

- The WUF-B assemblies with fully constrained beams failed due to local buckling followed by bolt shear rupture in the heating phase, with partial fracture of the flanges as a result of tensile forces developed in the cooling phase. The assemblies with unconstrained and partially constrained beams failed primarily due to shear rupture of the bolts. The peak axial compressive force in the beam for the unconstrained case was about one third of that for the fully constrained case and occurred at about three times the temperature.
- The RBS assemblies failed due to local buckling in the reduced section during the heating phase. The peak axial compressive force in the beam for the unconstrained case was about half of that for the fully constrained case and occurred at about four times the temperature.
- Tensile forces developed in the cooling phase only when plastic deformations occurred previously in the heating phase.
- All assemblies sustained the gravity loads without collapse, albeit with various degrees of damage.

Disclaimer

Certain commercial software or materials are identified to describe a procedure or concept adequately; such identification is not intended to imply recommendation, endorsement, or implication by the National Institute of Standards and Technology (NIST) that the software or materials are necessarily the best available for the purpose.

References

- American Institute of Steel Construction (AISC). (1999). *Load and resistance factor design specifications for structural steel buildings*. Chicago, IL.
- American Institute of Steel Construction (AISC). (2002). "Seismic provisions for structural steel buildings." *ANSI/AISC 341-02*, Chicago, IL.
- American Society of Civil Engineers (ASCE). (2002). "Minimum design loads for buildings and other structures." *SEI/ASCE 7-02*, Reston, VA.
- ASTM (2011), "ASTM Standard E119-11a Standard Test Methods for Fire Tests of Building Construction and Materials", *ASTM International*, West Conshohocken, PA, 2009, DOI: 10.1520/E0119-11A.
- Federal Emergency Management Agency (FEMA). (2000). "Recommended seismic design criteria for new steel moment-frame buildings." *FEMA 350*, SAC Joint Venture and FEMA, Washington, D.C.
- Hu, G., Morovat, M. A. (2009). "Elevated temperature properties of ASTM A992 steel." *ASCE- Structures Congress Proceedings*, 1067-1076.

- Kodur, V., Kand, S., and Khaliq, W. (2012). "Effect of Temperature on Thermal and Mechanical Properties of Steel Bolts." *Journal of Material in Civil Engineering*, 24(6), 765–774.
- Lew, H.S., Main, J.A., Robert, S.D., Sadek, F., and Chiarito, V.P. (2013). "Performance of steel moment connections under a column removal scenario. I: Experiments." *Journal of Structural Engineering*, ASCE, 139(1), 98-107.
- Livermore Software Technology Corporation (LSTC). (2012), "LS-DYNA Keyword User's Manual." Livermore, CA.
- Luecke, W. E., J.D. McColskey, C.N. McCowan, S.W. Banovic, R.J. Fields, T.J. Foecke, T.A. Siewert, F.W. Gayle (2005) "Federal Building and Fire Safety Investigation of the World Trade Center Disaster, Mechanical Properties of Structural Steels." *NIST NCSTAR 1-3D*, National Institute of Standards and Technology, Gaithersburg, MD.
- Luecke W., Gross J.L., McColskey J.D. (2014). "High-temperature, tensile, constitutive models for structural steel in fire", *AISC Engineering Journal*, (Submitted).
- Main, J.A, Sadek, F., (2012). "Robustness of steel gravity frame systems with single-plate shear connections." *NIST Technical Note 1749*, National Institute of Standards and Technology, Gaithersburg, MD.
- Quiel, S.E. and M.E.M. Garlock (2010) "Parameters for modeling a high-rise steel building frame subject to fire", *Journal of Structural Fire Engineering*, Vol 1, No. 2, pp 115-134.
- Research Council on Structural Connections (RCSC). (2004). Specifications for Structural Joints using ASTM A325 or A490 Bolts, AISC, Chicago.
- Sadek, F., Main, J., Lew, H., and El-Tawil, S. (2013). "Performance of Steel Moment Connections under a Column Removal Scenario. II: Analysis." *Journal of Structural Engineering*, ASCE, 139(1), 108–119.
- Sadek, F., Main, J.A., Lew, H.S., Robert, S.D., Chiarito, V.P., El-Tawil, S. (2010). "An Experimental and Computational Study of Steel Moment Connections under a Column Removal Scenario." *NIST Technical Note 1669*, National Institute of Standards and Technology, Gaithersburg, MD.
- Sarraj, M., Burgess, I.W., Davison, J.B., Plank, R.J. (2007). "Finite element modeling of steel fin plate connections in fire", *fire Safety Journal*, Vol 42, pp 408-415.
- Seif, M., McAllister, T. (2013). "Performance of steel shear tab connections at elevated temperatures." *Proceedings of Structural Stability Research Council Annual Stability Conference*, SSRC 2013, p. 123-135.
- Seif, M., McAllister, T., Main J., and Luecke, W. (2014). "Modeling of moment connections for structural fire analyses." *Proceedings of Structural Stability Research Council Annual Stability Conference*, SSRC 2014, p. 626-642.
- Seif, M.S., McAllister, T.P., Main, J.A., Luecke, W. (2015) "Finite element modeling of structural steel component failure at elevated temperatures." *Engineering Structures*. (under journal review).
- Wallaert, J. J., Fisher, J. W., (1965). "Shear strength of high-strength bolts." *Journal of the Structural Division*, ASCE, 91, ST3, 99-125.
- Yang, K.C., Chen, S.J., Ho, M.C. (2009) "Behavior of beam-to-column moment connections under fire load" *Journal of Constructional Steel Research*, 65(7), 1520-1527.
- Yu, H., Burgess, I.W., Davison, J.B., Plank, R.J. (2009). "Experimental investigation of the behavior of fin plate connections in fire", *Journal of Constructional Steel Research*, Vol 65, pp 723-736.